UNMANNED AIRCRAFT SYSTEMS AND SATELLITE TECHNOLOGIES FOR TOPSOIL MAPPING IN PRECISION AGRICULTURE

A. V. Ragazzo[1,2*], A. Mei[1], G. Fontinovo[1]

[1] Institute of Atmospheric Pollution Research, National Research Council of Italy, 00015 Monterotondo, Italy - (alfonso.ragazzo, alessandro.mei, giuliano.fontinovo)@iia.cnr.it
[2] Department of Science and Technology for Humans and the Environment, Unit of Electronics for Sensor Systems, Campus Bio-Medico University of Rome, Via Alvaro del Portillo 21, 00128 Rome, Italy

KEY WORDS: UAS, satellite, soil, salinity, geostatistics, GIS, Precision Agriculture.

ABSTRACT:

The use of satellite/UAS technologies in Precision Agriculture (PA) is increasing significantly and the continuous need of such kind of technologies is generating a great economic impact. This study carried out results by using Unmanned Aircraft Systems (UAS) and Very Hight Resolution (VHR) satellite imagery for the estimation of topsoil variability. The purpose of this contribution concerns the data analysis over two Production Units by evaluating radiometric response along the surface (e.g., spectral index). Our results concern the integration of UAS and satellite, improving the estimation accuracy of soil homogeneous areas variability, over which to manage agricultural practices. The remote sensing data covered by bare soil were isolated from the vegetative matrix along the study area. Thus, by using a statistical approach through the correlation between remote imagery and specific indices, it could be possible to determine variability in each pedological context, determining the zoning over land plots. According to this, in absence of high-resolution proximal soil sensing instrumentation, remote sensing data analysis can provide preliminary information suitable to establish a weighted topsoil/subsoil sampling campaign.

1. INTRODUCTION

Food production chain has undergone considerable growth over the last few years, reflecting in a technological upgrading for agronomical practices such as irrigation, fertilization, pesticides, and seeds use (World Resources Institute, 1998). Nowadays, Precision Agriculture (PA) techniques are able to achieve the following goals: (a) understanding the spatial distribution of homogeneous areas within the Production Units; (b) suppling innovative techniques on agriculture, focusing the attention on resources and practises management (Mamo et al., 2003; Crookston, 2006). According to this, the use of satellite and Unmanned Aircraft System (UAS) in PA has gone through a significant improvement, especially for the retrieval of vegetation and soil characteristics (Aslan et al., 2022; Ubina et al., 2022; Singh et al., 2022). This study is focused on soil spectral indices spatial variability, being those the result of complex relations between biological, geological, pedological, agronomic, geographic, and anthropogenic factors. Research dataset retrieved from remote sensing is used to map, for example, soil characteristics, in order to point out parameters such as yields, drainage, fertility, salinity, and irrigation design (Radoglou-Grammatikis et al., 2020). According to this, such kind of observations are mainly derived by five principal requirements: (a) characteristics of camera and sensor equipment; (b) easy application and employment of sensors and camera; (c) non-destructive measurements; (d) efficiency to retrieve the soil properties; (e) utilization of Structure from Motion (SfM) technique by computer vision approaches. According to this, user-friendly software are able to extract different kind of parameters such as canopies elevation and terrain modelling (Williams, 2012).

The aim of this contribution is to detect soil variability in order to pilot on-site pedological sampling. Indeed, site-specific soil characterization can be helpful for crop management on pre-planting and post-planting, thanks to the consideration and definition of physicochemical local variabilities (Larson et al., 1991; Costantini, 2007). Then, in terms of preliminary/not-invasive techniques, the utilization of satellite/UAS imageries can allow to obtain different information about the characterization of homogeneous areas in relation to the physicochemical topsoil variability (Douaoui et al., 2006; Castaldi et al., 2014; 2016; Colombo et al., 2015; Mei et al., 2020; Benedetti et al., 2021). Furthermore, homogeneous areas identification can occur by an integrated optical/radiometric sensor with visible and near-infrared spectral range (Viscarra Rossel et al., 2010). Hence, to highlight the homogeneous areas on bare soil, reflectance values will be associated with considerable presence of soil salinity and, consequently, with high values for spectral indices, such as Brightness Index (BI) or Salinity Index (SI) (Douaoui et al., 2006). Finally, the advancement of efficient and sustainable agricultural Site-Specific Crop Management (SSCM) policies is achievable by an high-speed and detailed spatial understanding of soil properties, which is essential to schedule local based Decision Support System (DSS) and develop Agriculture 4.0 advances.

2. MATERIAL AND METHODS

2.1 Study area

The area of interest is in Gerace (RC), within the region Calabria (Italy), at the Barone G.R. Macrì Agriculture Company. The study area is placed at an altitude about of 200 m.a.s.l., on the south-eastern side of the Calabrian Apennine. According to the sheet CARG 590 (Sheet CARG 590 "Taurianova" of the Geological Map of Italy at 1:50.000 scale), the geological formations that characterize the area are represented exclusively by sedimentary lithotypes. These are represented by the Apennine-Maghrebid orogen unit (Argille Variegate group-AV), the Terrigenous Miocene succession (Pier Niceto formation-PCT) and Clastic-Evaporitic Messinian succession (Vinco's Calcarenite-VNI). Then, the outcrops are represented by the following lithotype Units: pelite, matrix enclosing quartzarenite, arkose and limestone–Unit($_1$); marine-transitional pre-evaporitic pelite, limestone–gypsum unit, and coarse-grained alluvial-fan conglomerates–Unit($_2$), and sandy shallow-marine to continental progradational–Unit($_3$) (Sheet

CARG 590 "Taurianova" of the Geological Map of Italy at 1:50.000 scale; Cavazza et al., 1997; 2005). Regarding to the study area, the Production Units (PUs) are located in a north-south exposed area sheltered from sea winds by east ridges and characterized by several varieties of grape-vines implantation such as the Greco Bianco and the Greco Nero. According to the Calabrian Soil Chart, in the area of interest occur soil such as Cambisol, Calcisol, Luvisol, Regosol and Vertisol (Carta Dei Suoli Della Calabria - Scala 1:250.000). About the climate conditions, the Csa class (Hot Summer Mediterranean Climate) occurred, where summers tend to be hot and dry while winters relatively mild (Köppen, 1936). The annual averages of temperature, precipitation, and evapotranspiration measure 18.4 °C, 61.2 mm, and 87.3 mm respectively (ARPAC, 2022)
According to the Soil Map of Calabria (1:250000 scale), the study area concerns to the Soil Region 62.3, which includes alluvial and coastal plains. In details, the study area lies in the Soil Subregion 8, which is related to the Hilly environment of the Tyrrhenian slope, characterized, at elevations below 300 m.a.s.l., by moderately steep to steep slopes (6-35%). On turn, the previous Soil Subregion is subdivided by three soil units such as (1) slopes with different acclivity, (2) old terraces and (3) alluvial/colluvial deposits. Thus, in the study area occur the Soil Sub-System units 6.3 and 6.6, those correspond to landscapes with hummocky hills morphology with pelitic/silty deposits of Pliocene (Figure 1) and miocenic chaotic pelites.

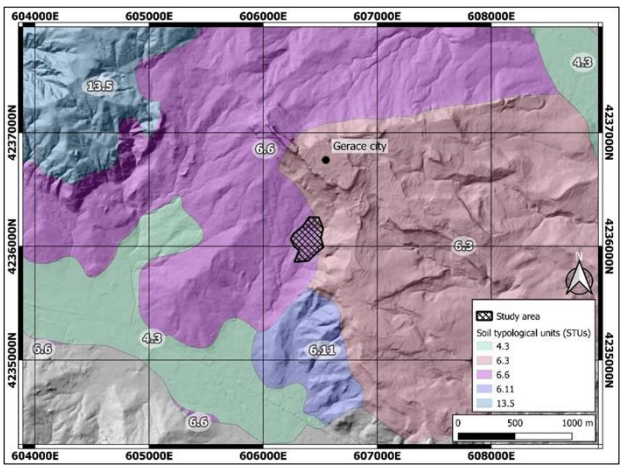

Figure 1. This image represents the Soil Typological Units (STUs) that characterize the Gerace study area (6.3 and 6.6).

Soil parent materials appertain to Pliocene and Quaternary sediments, exhibiting the absence or presence of carbonates, sub-acid to alkaline pH, and fine to coarse textures.
According to this, cartographic unit 6.3 is constituted by the following soil typological units (STUs):
• VIA_1: Ap-BCg-Cg, thin to moderately deep profile, no coarse fragments, fine texture, strongly alkaline, strongly calcareous, medium to high-water capacity, and slow drainage [Haplic-Gleyic Regosols].
• SAL_1: Ap-Bw-BCg-Cg, moderately deep profile, no coarse fragments, fine texture, alkaline, strongly calcareous, high-water capacity, and medium drainage [Haplic Calcaric Cambisols].
• GUA_1: Ap-Bk-Ckg, deep profile, no coarse fragments, fine texture, alkaline, strongly calcareous, high-water capacity, medium drainage, and medium tendency to crack during the dry season [Haplic Calcisols].
The cartographic unit 6.6 is constituted by the following STUs:
• CAO_1: A-BC-Cg, thin profile, from common to frequent coarse fragments, fine textures, alkaline to strong alkaline, slightly saline, low water capacity, and slow drainage [Calcaric-Hyposodic Regosols].

2.2 Instrumentation

2.2.1 Satellite

A programmed acquisition of WorldView3 satellite multispectral image is used for the study area investigation, concerning a spatial resolution of 1,24 m. The radiance data have been converted into reflectance during the operations in the atmospheric correction, applied through the ENVI® FLAASH module. However, spectral characteristics present a complex mixture of radiometric contributions among which can deriving, for example, from vegetation, shadows, environmental factors, colour and soil moisture. The data was processed in QGIS ambient, an open-source program that allows calculations and thematic maps elaboration. By using satellite images, Salinity Index 2 (SI2) and Brightness Index 2 (BI2) were computed in order to take into account the characteristics of soil and to obtain thematic maps.

2.2.2 UAS

Simultaneously with satellite acquisition, flights were carried out using Unmanned Aircraft System (UAS), in order to obtain different categories of information. So, overflights were carried out using a DJI Phantom 4 drone equipped with a Parrot Sequoia+ sensor that provide reflectance measurements. De facto, the Parrot Sequoia+ system concerns four multispectral sensors (Green, Red, Red-Edge, NIR) and a RGB camera, with a spatial resolution of 4 cm and 1 cm respectively. The use of a high resolution RGB camera made it possible to process the data in order to create a reference orthophoto, 3D models, and Digital Elevation Models (DEMs). About the multispectral sensor, green, red, red-edge, and near-infrared bands are characterized by the central wavelength corresponding to 550, 660, 735, 790 nm, respectively. Spectral resolution corresponds to 40 nm for Green, Red and Near-Infrared Bands, instead 10 nm for the Red-edge band. The focal length is 3.98 mm, the image size 1280 x 960 pixels, and the sensor size corresponds to 4.8 x 3.6 mm. Primarily, spectral calibration occurs with high reflective ground panels, secondly, through a sunshine sensor within the camera that can directly records and corrects the illumination information of each image. The flight mission was conducted with the following flight parameters: (a) flight altitudes (30 m.a.s.l.); (b) 80% front/side image overlap ratio; (c) flying speed 5 m/s.

2.3 Data processing

Photogrammetric data were processed in Agisoft Metashape version 2.0.1 (Agisoft LLC., St. Petersburg, Russia). So, from a set of overlapping images with the corresponding referenced information, a georeferenced dense point cloud was obtained. A dataframe was processed and analysed through algorithms integrated on Geographic Information System such as the Quantum GIS (QGIS) version 3.18.3 and ENVI version 5.3.1. Furthermore, statistical data were elaborated with R software (open-source), from which is used the following shared package in the CRAN (Comprehensive R Archive Network) platform: "PerformanceAnalytics".

Indices	Equation	Ref.
Excess Green (ExG)	$2*\left(\frac{B2}{B3+B2+B1}\right)-\left(\frac{B3}{B3+B2+B1}\right)-\left(\frac{B1}{B3+B2+B1}\right)$	[Rouse et al., 1974]
Salinity Index (SI)	$\sqrt{B2^2 * B3^2}$	[Douaoui et al., 2006]
Brightness Index (BI)	$\sqrt{(B2^2 * B3^2)/2}$	[Escadafal, 1989]
Salinity Index 2 (SI2)	$\sqrt{(B2^2 + B3^2 + B4^2)}$	[Douaoui et al., 2006]
Brightness Index 2 (BI2)	$\sqrt{B3^2 + B4^2}$	[Khan et al., 2001]

Table 1. List of spectral indices used in this paper for soil monitoring (B1 = Blue band; B2 = Green band; B3 = Red band, B4 = NIR).

In this study, the spectral indices were extracted from UAS derived orthophoto and UAS/satellite derived multispectral images. Spectral indices, listed in table 1, are based on remote sensing RGB/multispectral images, that are characterized by different spatial resolutions. The ExG spectral index is useful to create, firstly, a classification layer that can be suitable to separate soil from vegetation. Regarding the UAS data processing, by using ExG it was possible to isolate soil from vegetation by using the combination with a threshold layer, according to the studies related on the Otsu threshold value (Otsu, 1979). Hence, a threshold layer of soil was obtained through the raster calculation function, imposing values lower than 0.025 as characteristic of soil matrix. Finally, the Salinity Index (SI), Brightness Index (BI), Salinity Index 2 (SI2), and Brightness Index 2 (BI2) were used to highlight the homogeneous areas distribution along PUs (Figure 4).
Instead, radiometric data have been elaborated through stationary stochastic non-deterministic processes assuming normally distributed data (Matheron, 1963). According to this, the Ordinary CoKriging (OCK) method is chosen for the elaboration and spatialization of data, calculating automatically parameters through simulations. Then, OCK is a variation of the ordinary Kriging method, useful when there are close relationships between the spatial distributions of various known parameters (Aumond et al., 2018). This method concerns the determination of an empirical semivariogram, related to the spatial relationship dependences among primary data (autocorrelation) and primary to secondary variable (cross-correlation) (Myers, 1982). Semivariograms occur to measure unknown points, to fit models and to represent predicted data values. OCK model includes cross-validation of data, involving in the removal of each single sample point from the dataset and the consequent re-estimation of their values (Li et al., 2011).

2.3.1 Equations

To manage UAS and satellite data about topsoil, radiometric data extraction takes place. De facto, according to the equation (1), interpolation of points data and the nearest pixels through 1.5- and 3-meter circle buffer occurred (UAS and satellite respectively) , with the aim to remain consistent in relation to the field location accuracy.

$$z_\mu^*(x_0) = \mu_{ij}(x_n) \quad (1)$$

where $z_\mu^*(x_0)$ is the matrix derived from the buffering operation for the point (x0), containing the mean (μ) values related to each *j*-indexed parameter for each point (x_n) and each *i* statistical unit.

Consequently, according to Douaoui et al. (2006), correlation and calibration between UAS and satellite parameters related to the topsoil permit us to obtain a new salinity soil retrieval index. Indeed, through a statistical approach (regression and significance of the model), the correlation analysis between radiometric data (SI, BI, SI2, BI2) are employed in this study, in order to refine and raise the accuracy and trustworthiness of data acquired by satellite (Figure 2). Then, by means of simple regression method (SR) and calibration method (CL), in the following equations (2 and 3) are represented the retrieved spectral indices (RSIndex) as independent variable and ground data as dependent variable.

$$z^*_{SR}(s_0) = f\,[\mathrm{RSIndex}(s_0)] \quad (2)$$

where $z^*_{SR}(s_0)$ correspond to the value of the simple regression for the point (s_0), f is the regression function and RSIndex is the value of the spectral index for the point (s_0).

Finally, through the equation 3, a new spectral index will be obtained thanks to calibration operations between UAS and RSIndex data.

$$z^*_{CL}(s_0) = 0.61x + 0.10 \quad (3)$$

where $z^*_{CL}(s_0)$ is the calibrated RSIndex radiometric data obtained through the correction with UAS radiometric measurements by using linear correlation operations.

3. RESULTS AND DISCUSSION

BI rgb	SI rgb	BI2 mlt	SI2 mlt	BI2 wv	SI2 wv
0,53891	0,17437	0,23058	0,07705	0,15258	0,15620
0,52820	0,17345	0,24732	0,26466	0,23611	0,24341
0,75405	0,29154	0,29834	0,32216	0,28895	0,30633
0,47337	0,12840	0,27742	0,28895	0,27051	0,27554
0,63322	0,23740	0,26283	0,27477	0,24388	0,25256
0,88689	0,44919	0,27317	0,30150	0,31258	0,33378
0,69895	0,30443	0,31135	0,34148	0,26949	0,28368
0,53791	0,17139	0,30013	0,31343	0,2748	0,28409
0,67144	0,24291	0,26413	0,27579	0,24411	0,25154
0,69954	0,24953	0,23050	0,24866	0,2418	0,25224
0,64793	0,20934	0,27533	0,30251	0,26591	0,28201
0,83704	0,38521	0,27132	0,29239	0,28851	0,30251
0,57685	0,19661	0,26285	0,27856	0,25427	0,26324
0,82444	0,39211	0,33165	0,35853	0,31793	0,33952
0,78739	0,33382	0,27085	0,28718	0,27450	0,28530
0,82734	0,37577	0,26976	0,29054	0,26778	0,27974

ANOVA regression statistics	
Observations	16
Multiple R	0,90
R square	0,80
Adjusted R square	0,80
Standard Error	0,02
p-value	0,3E-05

Table 2. Summary output of regression statistics. rgb=UAS-RGB data (1cm spatial resolution); mlt=UAS multispectral data (4cm spatial resolution); wv= WorldView multispectral data (1.2m spatial resolution).

Observations between UAS (RGB and multispectral) and satellite data have been established, firstly, through a statistical method and, consequently, through a geostatistical approach. The best fitting between radiometric data occur between the SI2_mlt and SI2_wv indices. By using the R-Studio software a correlation matrix of the dataset in Table 2 is obtained. The plots in figure 2 are the results of a correlation between each statistical index (SI, BI, SI2, BI2). Furthermore, thanks to the assessment of descriptive and inferential statistical indices, such

as the linear correlation degree (r), the determination coefficient (R^2) and the significance degree (p-value), it was possible to establish that SI and SI2 spectral indices are the more relatable parameters regarding the highest values of r, R^2, and p-value (Figure 2). Indeed, as shown in table 1, the following values occur: 0.90, 0.81 and 0,3E-05 respectively (Table 2).

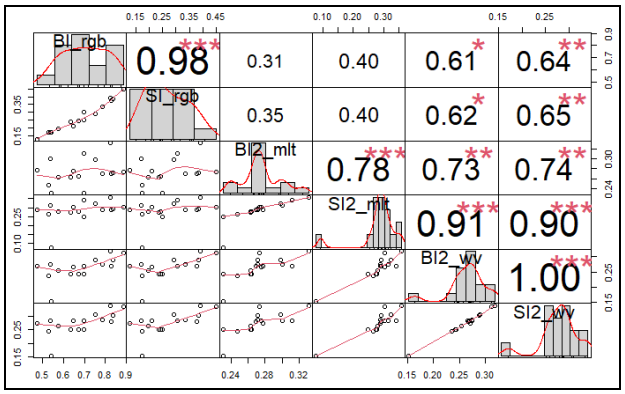

Figure 2. This image represent the results of correlation operation between the spectral indices by using the R package PerformanceAnalytics.

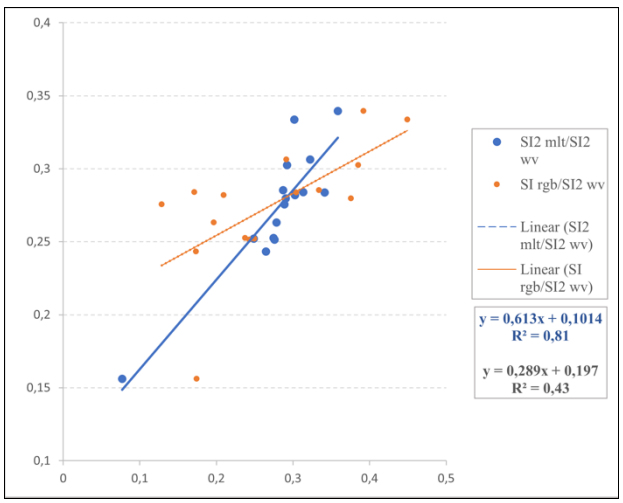

Figure 3. Visualization of the linear correlation line between SI rgb, SI2 mlt, and SI2 wv spectral indices.

Salinity map, obtained by the application of equations (2-3) and statistical approaches (Figure 2 and 3), serves to identify homogeneous areas along the topsoil surface. This kind of approach can permit to manage agronomical practices through the knowledge of homogeneous areas distribution. In figure 4 is shown a simple categorization of the area derived by the relation of radiometric data from UAS (RGB and multispectral) and satellite survey. According to this, the obtained spectral index z*CL (Table 3 and Figure 4) shows patches with high values in the west-southern part of the PUs of our interest, following a N-S oriented pattern, where lowest values characterize the north-eastern part of the parcel in exam. Finally, a OCK prediction map along PUs represents the spatialization of the radiometric spectral index z*CL, obtained from rectification with RGB/multispectral UAS acquisitions and WorldView3 satellite imagery.

ID		z*CL	
14	22	0,148632	0,270459
15	23	0,263637	0,253829
16	24	0,298884	0,286839
17	27	0,278526	0,280635
18	29	0,269834	0,272157
19	30	0,28622	0,321179
20	31	0,310727	0,277441
21	32	0,293533	0,279501

Table 3. Dataframe related to the new correlate spectral index obtained by statistic operations.

The prediction map has been obtained from a statistical and geostatistical approach as the Ordinary Cokriging method. As is shown in the figure 4, two main soil homogeneous areas are noticeable, concerning variability on salinity content from low-medium to high-medium quality. In the end, the results can be useful for manage agricultural practices in PA, using further correlation between the obtained soil thematic map and eventual thematic maps related to the main vegetation parameters' characteristics.

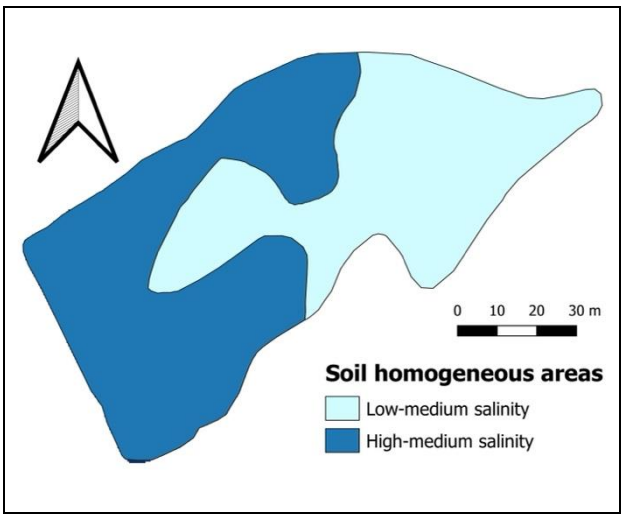

Figure 4. Visualization of OCK prediction map representing the study area. The spatialization of the obtained spectral index z*CL occurred from UAS and satellite data (SI rgb, SI2 mlt, and SI2 wv spectral indices).

4. CONCLUSION

This study deals with soil salinity mapping and monitoring, based on RGB/multispectral UAS and satellite images. The findings of this study prove that different technologies, such as UAS and satellite, have a good degree of correlation. According to this, it has been possible to calibrate the pixel matrix (1.2 meter of spatial resolution) from the satellite with the high resolution pixel matrix acquired from UAS (1 to 4 cm of spatial resolution). Consequently, by data correlation/calibration operations, a more accurate satellite image was obtained. Indeed, a good data processing of remote sensing data can be fundamental to pilot in-situ soil sampling campaign as preliminary analysis for the detection of topsoil variability along land parcels. This study highlighted that SI and SI2 spectral indices may be used to enhance the saline patches along PUs, since best coefficient of correlation (R^2 = 0.81) between different resolution images from UAS and satellite occurred. Thus, a calibration model and spatial map of salinity has been

obtained with the aim to divided PUs into two homogenous areas on which an agricultural practises management can be applied. In the end, from this study is concluded that UAS data can support an extend spatial soil detection along land parcels by satellite imagery, with the aim to constitute a dataset of soil salinity useful for soil scientists, agronomists and farmers.

REFERENCES

Abdelkader, Douaoui & Nicolas, Hervé & Walter, Christian. (2006). Detecting salinity hazards within a semiarid context by means of combining soil and remote-sensing data. Geoderma. 134. 217-230. 10.1016/j.geoderma.2005.10.009.

Agenzia Regionale per la Protezione dell'Ambiente della Calabria - Via Lungomare (loc. Giovino) – 88100 Catanzaro.

Aslan, M. F., Durdu, A., Sabanci, K., Ropelewska, E., & Gültekin, S. S. (2022). A Comprehensive Survey of the Recent Studies with UAV for Precision Agriculture in Open Fields and Greenhouses. Applied Sciences, 12(3), 1047.

Aumond, Pierre & Can, Arnaud & Mallet, Vivien & De Coensel, Bert & Ribeiro, Carlos & Botteldooren, Dick & Lavandier, Catherine. (2018). Kriging-based spatial interpolation from measurements for sound level mapping in urban areas. The Journal of the Acoustical Society of America. 143. 2847-2857. 10.1121/1.5034799.

Benedetti, F. and Caon, L. 2021. Global Soil Laboratory Assessment 2020 – Laboratories' capacities and needs. Rome, FAO.

Castaldi, F., Casa, R., Castrignanò, A., Pascucci, S., Palombo, A. and Pignatti, S. (2014), Estimation of soil properties at the field scale from satellite data: a comparison between spatial and non-spatial techniques. Eur J Soil Sci, 65: 842-851. https://doi.org/10.1111/ejss.12202.

Cavazza, W.; Blenkinsop, J; De Celles, P.G.; Patterson, R.T; Reinhardt, E.G. Stratigrafia e sedimentologia della sequenza sedimentaria oligocenica-quaternaria del bacino Calabro Ionico. Bollettino della Società Geologica Italiana, 1997, vol. 116, n. 1, pp 51-77.

Cavazza, W., Ingersoll, R.V., 2005. Detrital Modes of the Ionian forearc basin fill (Oligocene-Quaternary) reflect the tectonic evolution of the Calabria-Peloritani terrane (Southern Italy). Journal of Sedimentary Research 75, 268–279.

Castaldi, Fabio & Palombo, Angelo & Santini, Federico & Pascucci, Simone & Pignatti, Stefano & Casa, Raffaele. (2016). Evaluation of the potential of the current and forthcoming multispectral and hyperspectral imagers to estimate soil texture and organic carbon. Remote Sensing of Environment. 179. 54 - 65. 10.1016/j.rse.2016.03.025.

Colombo C., Miano T., 2015. Metodi di analisi chimica del suolo. Società italiana della scienza del suolo & Associazione Italiana dei Laboratori Pubblici di Agrochimica.

Crookston, K. (2006). A top 10 list of developments and issues impacting crop management and ecology during the past 50 years. Crop Science, 46.

Costantini E. A. C. (Ed.) 2007. Linee guida dei metodi di rilevamento e informatizzazione dei dati pedologici. CRA-ABP, Firenze, Italia, pp. XV, 280.

Abdelkader, Douaoui & Nicolas, Hervé & Walter, Christian. (2006). Detecting salinity hazards within a semiarid context by means of combining soil and remote-sensing data. Geoderma. 134. 217-230. 10.1016/j.geoderma.2005.10.009.

Escadafal, R. (1989). Remote sensing of arid soil surface color with Landsat thematic mapper. Advances in Space Research, 9:159-163.

Khan, S.A., Mulvaney, R.L. and Hoeft, R.G. (2001), A Simple Soil Test for Detecting Sites that are Nonresponsive to Nitrogen Fertilization. Soil Sci. Soc. Am. J., 65: 1751-1760.

Köppen, W. Das geographische System der Klimate, 1–44 (Gebrüder Borntraeger: Berlin, Germany, 1936).

Lamb, D., Hall, A., & Louis, J. (2001). Airborne remote sensing of vines for canopy variability and productivity. Australian Grapegrower and Winemaker, 89-94.

Larson, W.E., Robert, P.C., 1991. Agriculture by soil. In: Lal, R., Pierce, F.J. (Eds.), Soil Management for Sustainability. Soil and Water Conservation Society, Ankeny, IA, USA, pp. 103–112.

Li, J., Heap, A.D., 2011. A review of comparative studies of spatial interpolation methods in environmental sciences. Performance and impact factors. Ecol. Inf. 6 (3-4), 228–241.

Matheron, G. (1963) Principles of Geostatistics. Economic Geology, 58, 1246-1266. http://dx.doi.org/10.2113/gsecongeo.58.8.1246.

Mei A., Fontinovo G., Rantica E., Allegrini A. (2020) - Integration of satellite, UAV and field data for soil analysis in precision viticulture; Rend. Online Soc. Geol. It., Vol. 52 (2020), pp. 33-39.

Mamo, M., Malzer, G. L., Mulla, D. J., Huggins, D. J., & Strock, J. (2003). Spatial and temporal variation in economically op-timum N rate for corn. Agronomy Journal, 95, 958e964.

Myers, Donald. (1982). 1982, Myers,D.E., Matrix Formulation of Cokriging Mathematical Geology 14, 249-257. Mathematical Geology. 14. 249-257.

N. Otsu, "A Threshold Selection Method from Gray-Level Histograms," in IEEE Transactions on Systems, Man, and Cybernetics, vol. 9, no. 1, pp. 62-66, Jan. 1979, doi: 10.1109/TSMC.1979.4310076.

Radoglou-Grammatikis, P.; Sarigiannidis, P.; Lagkas, T.; Moscholios, I. A compilation of UAV applications for precision agriculture. Comput. Netw. 2020, 172, 107148.

Rouse, J.W.; Haas, R.H.; Schell, J.A.; Deering, D.W. Monitoring vegetation system in the great plains with ERTS. Proceedings of the Third Earth Resources Technology Satellite-1 Symposium, Greenbelt, USA; NASA SP-351, 1974; pp. 3010-3017.

Servizio Agropedologico della Calabria, Carta Dei Suoli a scala 1:250.000. ARSAC, 2003.

Servizio Geologico d'Italia (2015) - Carta Geologica d'Italia alla scala 1:50.000, F. 590 Taurianova. ISPRA, Roma.

Singh, A. P., Yerudkar, A., Mariani, V., Iannelli, L., & Glielmo, L. (2022). A Bibliometric Review of the Use of Unmanned Aerial Vehicles in Precision Agriculture and Precision Viticulture for Sensing Applications. Remote Sensing, 14(7), 1604.

Ubina NA, Cheng S-C. A Review of Unmanned System Technologies with Its Application to Aquaculture Farm Monitoring and Management. Drones. 2022; 6(1):12

Viscarra Rossel R.A., Walvoort D.J.J., McBratney A.B., Janik L.J. & Skjemstad J.O. (2006) Visible, near infrared, mid infrared or combined diffuse reflectance spectroscopy for simultaneous assessment of various soil properties. Geoderma, 131, 59–75.

Williams, R.D. (2012). DEMs of difference.

World Resources Institute, 1998. 1998–99 World Resources – A Guide to the Global Environment. Oxford University Press, New York, USA.